

Reduced cross section and gluon distribution in momentum-space approach

G.R. Boroun*

Department of Physics, Razi University, Kermanshah 67149, Iran

Phuoc Ha†

Department of Physics, Astronomy and Geosciences, Towson University, Towson, MD 21252

(Dated: February 12, 2025)

We present a calculation of the reduced cross section in momentum-space approach utilizing the Block-Durand-Ha (BDH) parameterization of the proton structure function $F_2(x, Q^2)$ and the leading-order (LO) longitudinal structure function $F_L(x, Q^2)$, proposed by Boroun and Ha [G.R. Boroun and P.Ha, Phys. Rev. D **109** (2024) 094037] using Laplace transform techniques. Our results are compared with the HERA data and extended to the Large Hadron electron Collider (LHeC) domain. We also examine the ratio $F_{L2}(x, Q^2) = F_L(x, Q^2)/F_2(x, Q^2)$ obtained from our work, comparing it with both the H1 data and the color dipole (CDP) bounds. We find that our results for the reduced cross section and the ratio $F_{L2}(x, Q^2)$ agree with the H1 data. Finally, our evaluation of the gluon distribution functions $G(x, Q^2)$ in momentum-space approach shows very good concordance with the NNPDF3.0LO gluon structure functions for moderate Q^2 in the range $10^{-5} \leq x \leq 1$.

INTRODUCTION

One of the ways to understand and explore the dynamics of strong interactions and test Quantum Chromodynamics (QCD) is through measurements of the inclusive deep inelastic lepton-nucleon scattering (DIS) cross-section [1]. The HERA accelerator, which went through different phases known as HERA I and HERA II, operated from 1992 to 2007 at DESY in Hamburg. During this time, electrons or positrons collided with protons at a center-of-mass energy $\sqrt{s}=320$ GeV. Specifically, one storage ring accelerated electrons to energies of 27.6 GeV, while the other accelerated protons to energies of 920 GeV in the opposite direction. HERA played a crucial role in studying proton structure and quark properties, laying the groundwork for research at the Large Hadron Collider (LHC) at CERN. HERA kinematics cover the values of Bjorken- x in the interval $10^{-5} \lesssim x < 1$ and Q^2 , the squared four-momentum transfer between lepton and nucleon, in the interval $0.1 \text{ GeV}^2 \lesssim Q^2 \lesssim 1000 \text{ GeV}^2$ [2]. These measurements can be performed with much increased precision and extended to much lower values of x and high Q^2 in next ep colliders. These new colliders under design are the Large Hadron electron Collider [3] with center-of-mass energy $\sqrt{s} \simeq 1.3$ TeV and the Future Circular Collider electron-hadron (FCC-eh) [3, 4] with $\sqrt{s}=3.5$ TeV. The center-of-mass energy at the LHeC is about 4 times of the center-of-mass energy range of ep collisions at HERA and the kinematic range in the (x, Q^2) plane in neutral-current (NC) extends below $x \approx 10^{-6}$ and up to $Q \simeq 1$ TeV and will be extended down to $x \approx 10^{-7}$ at the FCC-eh program [3–8].

The measurements at HERA for the longitudinal structure function have been performed with the extrapolation and derivative methods at large and low Q^2 values [1]. At HERA, the longitudinal structure function can be extracted from the inclusive cross section only in the region of large inelasticity with $y = Q^2/sx$, where y is the inelasticity variable. Here x and Q^2 are two independent kinematic variables and s is the center of mass energy squared. The reduced cross section, in the inclusive DIS scattering, is defined in terms of the two proton structure functions $F_2(x, Q^2)$ and $F_L(x, Q^2)$ as

$$\sigma_r = F_2(x, Q^2) - \frac{y^2}{1 + (1 - y)^2} F_L(x, Q^2) = F_2(x, Q^2) \left[1 - \frac{y^2}{1 + (1 - y)^2} F_{L2}(x, Q^2) \right], \quad (1)$$

*Electronic address: boroun@razi.ac.ir

†pdha@towson.edu

where $F_{L2} = F_L/F_2$. The ratio F_{L2} can be defined into the cross section ratio R by the following form

$$F_{L2}(x, Q^2) = \frac{F_L(x, Q^2)}{F_2(x, Q^2)} = \frac{R(x, Q^2)}{1 + R(x, Q^2)}, \quad (2)$$

where R is related to the cross sections σ_T and σ_L for absorption of transversely or longitudinally polarised virtual photons as

$$R(x, Q^2) = \frac{\sigma_L^{\gamma^* p}(x, Q^2)}{\sigma_T^{\gamma^* p}(x, Q^2)}. \quad (3)$$

In this paper, we present a calculation of the reduced cross section in momentum-space approach using the Block-Durand-Ha (BDH) parameterization¹ of the proton structure function $F_2(x, Q^2)$ [9] and the LO longitudinal structure function $F_L(x, Q^2)$, proposed by Boroun and Ha (BH) [10] using Laplace transform techniques [11–14]. We then compare our results of the reduced cross section in the momentum-space approach with the H1 data [15] and extend the results to the LHeC domain [3]. Additionally, we investigate the ratio $F_{L2}(x, Q^2)$ obtained from our work, comparing it with both the H1 data and the color dipole picture (CDP) bounds². We also evaluate the gluon distribution function in the momentum-space approach, and compare our results with those in set NNPDF3.0³ of the NNPDF Collaboration of Ball *et. al* [16].

REDUCED CROSS SECTION IN MOMENTUM-SPACE APPROACH

The authors in Ref.[9] have obtained the BDH parameterization of the structure function $F_2(x, Q^2)$, from a combined fit to HERA data. The explicit expression takes the following form

$$F_2^{\text{BDH}}(x, Q^2) = D(Q^2)(1-x)^n \sum_{m=0}^2 A_m(Q^2) L^m, \quad (4)$$

with

$$\begin{aligned} D(Q^2) &= \frac{Q^2(Q^2 + \lambda M^2)}{(Q^2 + M^2)^2}, \quad A_0 = a_{00} + a_{01}L_2, \quad A_i(Q^2) = \sum_{k=0}^2 a_{ik}L_2^k, \quad (i = 1, 2), \\ L &= \ln(1/x) + L_1, \quad L_1 = \ln \frac{Q^2}{Q^2 + \mu^2}, \quad L_2 = \ln \frac{Q^2 + \mu^2}{\mu^2}, \end{aligned} \quad (5)$$

where the effective parameters are summarized in Ref.[33] and are given in Table I.

In a recent paper [10], using Laplace transform techniques [11–14], we have determined the longitudinal structure function $F_L(x, Q^2)$, at the leading-order approximation in momentum-space approach⁴, from the proton structure

¹ The BDH parameterization provides a better fit to experimental data, particularly at low values of the Bjorken variable x . This improved fit is crucial for accurately describing the behavior of the proton structure function in regions where data is sparse. Additionally, the BDH parameterization aligns well with theoretical predictions, such as the Froissart bound, which describes the asymptotic behavior of hadron-hadron cross sections. By avoiding the need for a specific factorization scheme, the BDH parameterization simplifies the theoretical calculations involved in deep inelastic scattering processes, making them more efficient and accessible.

² For further discussion please refer to Appendix A.

³ The NNPDF3.0 is the first set of parton distribution functions owing to HERA, ATLAS, CMS and LHCb data based on LO, NLO and NNLO QCD theory.

⁴ The momentum-space approach has two advantages:

1) It is no need to define a factorization scheme,
2) The approach in terms of physical structure functions has the advantage of being more transparent in the parametrization of the initial conditions of the evolution.

function and its derivative with respect to $\ln Q^2$ as

$$\begin{aligned}
F_L^{\text{BH}}(x, Q^2) = & 4 \int_x^1 \frac{dF_2^{\text{BDH}}(z, Q^2)}{d\ln Q^2} \left(\frac{x}{z}\right)^{3/2} \left[\cos\left(\frac{\sqrt{7}}{2} \ln \frac{z}{x}\right) - \frac{\sqrt{7}}{7} \sin\left(\frac{\sqrt{7}}{2} \ln \frac{z}{x}\right) \right] \frac{dz}{z} - 4C_F \frac{\alpha_s(Q^2)}{2\pi} \\
& \times \int_x^1 F_2^{\text{BDH}}(z, Q^2) \left(\frac{x}{z}\right)^{3/2} \left[(1.6817 + 2\psi(1)) \cos\left(\frac{\sqrt{7}}{2} \ln \frac{z}{x}\right) + (2.9542 - 2\frac{\sqrt{7}}{7}\psi(1)) \sin\left(\frac{\sqrt{7}}{2} \ln \frac{z}{x}\right) \right] \frac{dz}{z} \\
& + 8C_F \frac{\alpha_s(Q^2)}{2\pi} \sum_{k=1}^{\infty} \frac{k}{(k+1)^2 - 3(k+1) + 4} \int_x^1 F_2^{\text{BDH}}(z, Q^2) \left(\frac{x}{z}\right)^{k+1} \frac{dz}{z}. \quad (6)
\end{aligned}$$

As shown in the Appendix B, the last term in Eq. (6) can be modified to improve the convergence substantially for increasing numbers of terms in the series. Therefore, the momentum space evolution of the longitudinal structure function $F_L^{\text{BH}}(x, Q^2)$ can then be written as

$$\begin{aligned}
F_L^{\text{BH}}(x, Q^2) = & 4 \int_x^1 \frac{dF_2^{\text{BDH}}(z, Q^2)}{d\ln Q^2} \left(\frac{x}{z}\right)^{3/2} \left[\cos\left(\frac{\sqrt{7}}{2} \ln \frac{z}{x}\right) - \frac{\sqrt{7}}{7} \sin\left(\frac{\sqrt{7}}{2} \ln \frac{z}{x}\right) \right] \frac{dz}{z} - 4C_F \frac{\alpha_s(Q^2)}{2\pi} \\
& \times \int_x^1 F_2^{\text{BDH}}(z, Q^2) \left(\frac{x}{z}\right)^{3/2} \left[(1.6817 + 2\psi(1)) \cos\left(\frac{\sqrt{7}}{2} \ln \frac{z}{x}\right) + (2.9542 - 2\frac{\sqrt{7}}{7}\psi(1)) \sin\left(\frac{\sqrt{7}}{2} \ln \frac{z}{x}\right) \right] \frac{dz}{z} \\
& + 8C_F \frac{\alpha_s(Q^2)}{2\pi} \left[\sum_{m=1}^{\infty} \left(\frac{2(m-4)}{m(m^2 - 3m + 4)} - \frac{2}{m^2} \right) \int_x^1 F_2^{\text{BDH}}(z, Q^2) \left(\frac{x}{z}\right)^m \frac{dz}{z} \right. \\
& \left. + \int_x^1 F_2^{\text{BDH}}(z, Q^2) \left(\text{Li}_2\left(\frac{x}{z}\right) - \ln\left(1 - \frac{x}{z}\right) \right) \frac{dz}{z} \right]. \quad (7)
\end{aligned}$$

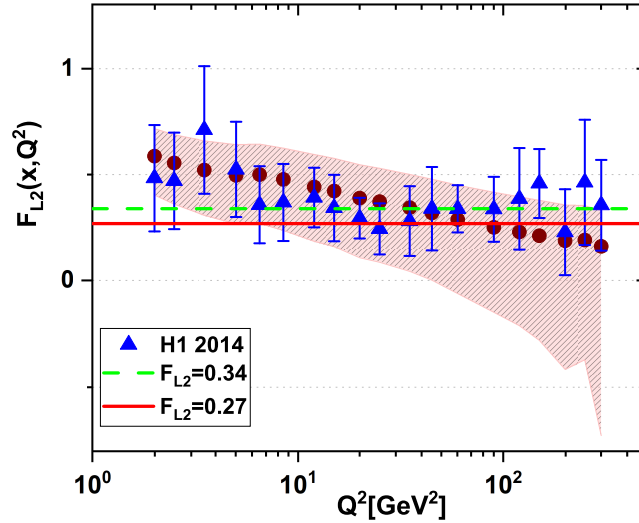


FIG. 1: The extracted ratio F_{L2} (shown as brown points) from the parametrization methods is compared with the H1 data [15]. The total errors are included, and the dipole upper bounds are represented by curves corresponding to $F_{L2} = 0.27$ (solid red line) and $F_{L2} = 0.34$ (dashed green line). The error bands (rose gold) of the ratio F_{L2} correspond to the uncertainty in the parameterization of $F_2(x, Q^2)$ in [9].

In Fig.1, we show the ratio of the structure functions based on the F_2 and F_L parametrizations in [9] and [10], respectively. The behavior of the ratio $F_{L2}(x, Q^2)$ is compared with the H1 data [15] and the CDP bounds. The H1 data are selected in the region $2 \leq Q^2 \leq 300 \text{ GeV}^2$ at the interval $156 \leq W \leq 233 \text{ GeV}$ with the maximum value of the

longitudinal structure function⁵. The values of the ratio of structure functions describe well the H1 data in the region $2 \leq Q^2 \leq 300 \text{ GeV}^2$ and they are in good agreement with the CDP bounds in the interval $5 \leq Q^2 \leq 300 \text{ GeV}^2$ as data on $F_{L2}(x, Q^2)$ confirm the standard dipole picture at these kinematic points. The error bars of the ratio F_{L2} (in H1 data and our method) are determined by the following form:

$$\Delta(F_{L2}) = F_{L2} \sqrt{(\Delta F_L/F_L)^2 + (\Delta F_2/F_2)^2},$$

where in the H1 data, ΔF_L and ΔF_2 are collected from the H1 experimental data [15]. In this paper, the error bands are dependent on the uncertainties of $F_2(x, Q^2)$ and $F_L(x, Q^2)$. The uncertainties in $F_2(x, Q^2)$ are obtained from the parametrization coefficients in the BDH model (Table I), while the uncertainties in $F_L(x, Q^2)$ are obtained through Eq.(7), which depends on the uncertainties in $F_2(x, Q^2)$.

The values of the ratio of structure functions are comparable with the H1 data and they are in good agreement with the CDP bounds in the interval $5 \leq Q^2 \leq 300 \text{ GeV}^2$ as data on $F_{L2}(x, Q^2)$ confirm the standard dipole picture at these kinematic points. In order to include the effect of production threshold for charm quark with $m_c = 1.29^{+0.077}_{-0.053} \text{ GeV}$ [15, 34], the rescaling variable χ is defined by the form $\chi = x(1 + 4\frac{m_c^2}{Q^2})$ where reduced to the Bjorken variable x at high Q^2 [34]. The rescaling variable is one of the ingredients used in the general-mass variable flavor number schemes (GM-VFNS)[35]. Using $\alpha_s(M_Z^2) = 0.1166$ and the leading-order (LO) form of $\alpha_s(Q^2)$, the QCD parameter Λ for four active flavors has been extracted [33], resulting in $\Lambda = 136.8 \text{ MeV}$.

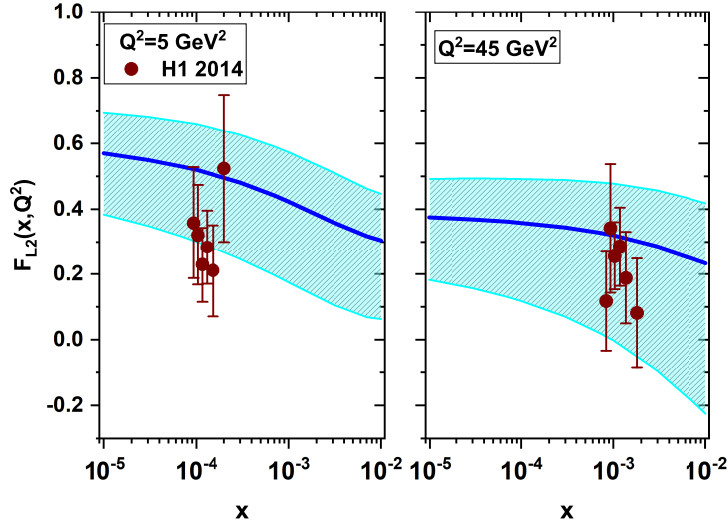


FIG. 2: The ratio of structure functions extracted (blue solid curve) in comparison with the H1 data [15] as accompanied with total errors. The results are presented at $Q^2 = 5$ and 45 GeV^2 in a wide range of x . The error (turquoise) bands correspond to the uncertainty in the parameterization of $F_2(x, Q^2)$ in [9].

In Fig. 2, the results for the ratio of structure functions, $F_{L2}(x, Q^2)$, at fixed values of $Q^2 = 5$ and 45 GeV^2 in a wide range of x are presented and compared with the H1 data [15] as accompanied with total errors. The error bands correspond to the uncertainty in the parameterization of $F_2(x, Q^2)$ in [9]. As seen in the figure, the results are comparable with the H1 data in a wide range of x . The extracted ratio of structure functions is in good agreement with the H1 data as accompanied with total errors.

The extracted results for the longitudinal structure function in momentum-space approach Ref.[10] are in line with data from the H1 Collaboration and other results using Mellin transform method [33]. In the following, the ratio $F_{L2}(x, Q^2) = F_L^{\text{BH}}(x, Q^2)/F_2^{\text{BDH}}(x, Q^2)$ is parametrized using the BDH parametrization of the proton structure

⁵ Please see Table 5 in Ref.[15]

function $F_2^{\text{BDH}}(x, Q^2)$ (i.e., Eq.(4)), and the reduced cross section is parametrized by

$$\sigma_r = F_2^{\text{BDH}}(x, Q^2) \left[1 - \frac{y^2}{1 + (1 - y)^2} F_{L2}(x, Q^2) \right]. \quad (8)$$

The calculation of the ratio of structure functions facilitates the accurate determination of the reduced cross section σ_r (i.e., Eq.(8)). The results of the reduced cross section σ_r are depicted in Fig.3 as the center-of-mass energy extended to the LHeC study group [4]. A comparison with the H1 data [1] is done as accompanied with total errors at moderate x and extended to the very low x due to the LHeC region with $y \leq 1$. These results for the reduced cross section reflect the large extension of kinematic range towards low x and high Q^2 available at the LHeC, as compared to HERA.

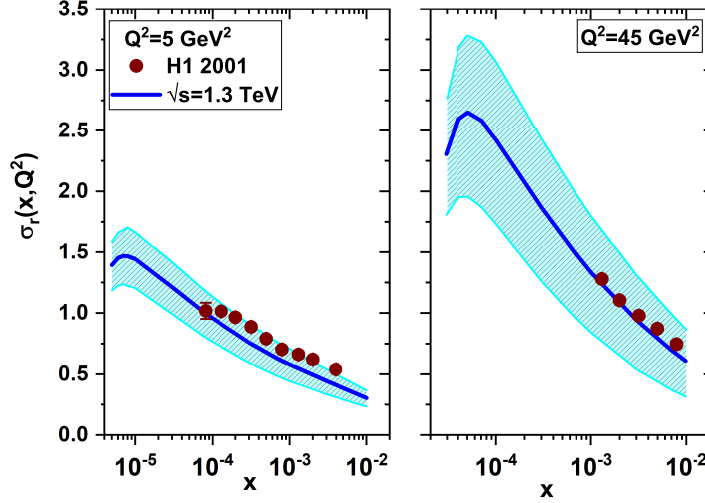


FIG. 3: The reduced cross section extracted (blue solid curve) in comparison with the H1 data [1] as accompanied with total errors. The results are presented and extended to the center-of-mass energy of the LHeC, $\sqrt{s} = 1.3$ TeV with $y < 1$ at $Q^2 = 5$ and 45 GeV^2 . The error (turquoise) bands correspond to the uncertainty in the parameterization of $F_2(x, Q^2)$ in [9]

GLUON DISTRIBUTION IN MOMENTUM-SPACE APPROACH

The gluonic density, in high-energy scattering processes, exhibits a crucial phenomenon at the small- x region and plays a vital role in estimating backgrounds. At low values of x , the structure functions $F_2(x, Q^2)$ and $F_L(x, Q^2)$ are defined solely via the singlet quark $x\Sigma(x, Q^2)$ and gluon distribution $xg(x, Q^2)$ as

$$F_k(x, Q^2) = \langle e^2 \rangle \left[B_{k,s}(x, \alpha_s(Q^2)) \otimes x\Sigma(x, Q^2) + B_{k,g}(x, \alpha_s(Q^2)) \otimes xg(x, Q^2) \right], \quad k = 2, L$$

where $\langle e^2 \rangle$ is the average charge squared for the number of effective flavours and $\alpha_s(Q^2)$ is the running coupling. The quantities $B_{k,a}(x)$ are the known Wilson coefficient functions and the parton densities fulfil the renormalization group evolution equations⁶.

The gluon density in the momentum-space approach contributes to the DIS structure functions F_2 and F_L as defined in [36] by the following formula:

$$g(x, Q^2) = \int_x^1 \frac{dz}{z} \delta(1 - z) \left\{ \eta \left[\frac{x}{z} \frac{d}{dz} - 2 \right] \frac{F_2(\frac{x}{z}, Q^2)}{\frac{x}{z}} + \zeta \left[\frac{x^2}{z^2} \frac{d^2}{d(\frac{x}{z})^2} - 2 \frac{x}{z} \frac{d}{dz} + 2 \right] \frac{F_L(\frac{x}{z}, Q^2)}{\frac{x}{z} \frac{\alpha_s(Q^2)}{2\pi}} \right\}, \quad (9)$$

⁶ Here the non-singlet densities become negligibly small in comparison with the singlet densities. The symbol \otimes indicates convolution over the variable x by the usual form, $f(x) \otimes g(x) = \int_x^1 \frac{dz}{z} f(z, \alpha_s) g(x/z)$.

where $\eta = C_F/(4T_R n_f < e^2 >)$ and $\zeta = 1/(8T_R n_f < e^2 >)$ with the color factors $T_R = 1/2$ and $C_F = 4/3$ associated with the color group SU(3).

After successive differentiations of the brackets in Eq. (9) with respect to $\frac{x}{z}$ and some rearranging, using the identity $\frac{x}{z} = y$, we find

$$g(x, Q^2) = \int_x^1 \frac{dy}{y} \delta(1 - \frac{x}{y}) \left\{ \eta \left[\frac{\partial F_2(y, Q^2)}{\partial y} - 3 \frac{F_2(y, Q^2)}{y} \right] + \zeta \frac{2\pi}{\alpha_s(Q^2)} \left[y \frac{\partial^2 F_L(y, Q^2)}{\partial^2 y} - 4 \frac{\partial F_L(y, Q^2)}{\partial y} + \frac{6}{y} F_L(y, Q^2) \right] \right\}. \quad (10)$$

Using the delta function property, we find the the momentum space evolution of the gluon distribution in terms of the structure functions as

$$G(x, Q^2) = \eta \left[x \frac{\partial F_2(x, Q^2)}{\partial x} - 3 F_2(x, Q^2) \right] + \zeta \frac{2\pi}{\alpha_s(Q^2)} \left[x^2 \frac{\partial^2 F_L(x, Q^2)}{\partial^2 x} - 4x \frac{\partial F_L(x, Q^2)}{\partial x} + 6 F_L(x, Q^2) \right], \quad (11)$$

where $G(x, Q^2) = xg(x, Q^2)$. This is a simple form of the gluon distribution, expressed through the parametrization of the proton structure function (i.e., Eq. (4)) and the longitudinal structure function (i.e., Eq. (7)) in momentum-space approach at low values of x . We note that the method of Lappi et al. [36], on which our work is based, (1) neglects non-singlet contributions and (2) is a high- Q^2 approximation. The results for the gluon distribution function (i.e. Eq.(11)) in the momentum-space approach are presented in Figs.4-5. These results are included with and without the rescaling variable, including the charm quark mass.

As can be seen in Fig.4, the results are comparable with the NNPDF3.0LO for $Q^2 = 10, 20, 50$, and 100 GeV^2

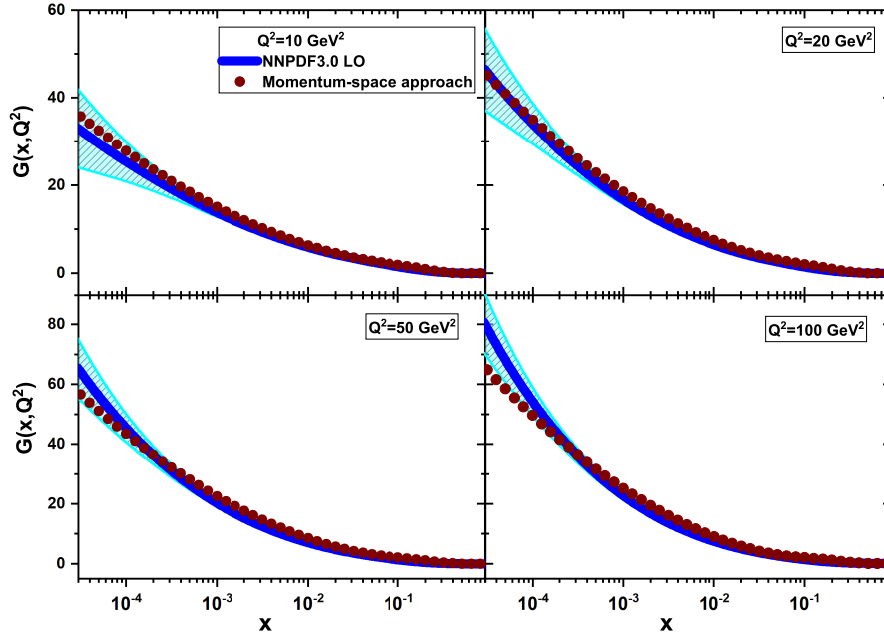


FIG. 4: The gluon distribution function $G(x, Q^2)$ (brown points) with considering the rescaling variable of x in the momentum-space approach extracted and compared with the NNPDF3.0LO [16] as accompanied with total errors (turquoise bands) for $Q^2 = 10, 20, 50$, and 100 GeV^2 in a wide range of x .

in a wide range of x with the rescaling variable of x . Notably, the values of the gluon distribution function increase as x decreases, a trend that is in harmony with the expectations of pQCD. The results of $G(x, Q^2)$ based on the momentum-space approach show very good agreement with the NNPDF3.0LO gluon structure function for moderate Q^2 in the range $10^{-5} \leq x \leq 1$. The comparison between the results (i.e., momentum-space approach

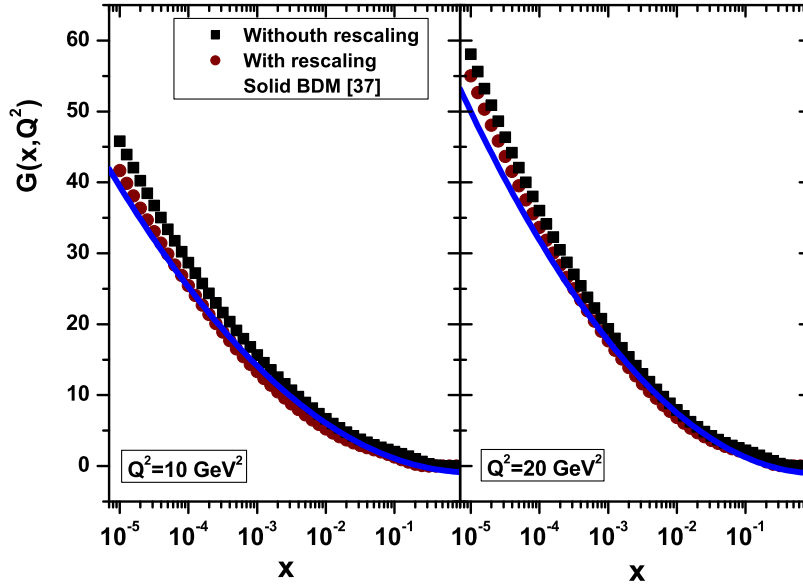


FIG. 5: The gluon distribution function $G(x, Q^2)$ with (brown points) and without (black points) rescaling variable in the momentum-space approach extracted and compared with the BDM result [37] (blue curve) for $Q^2 = 10$, and 20 GeV^2 in a wide range of x .

and NNPDF3.0LO) with the rescaling variable at $Q^2 = 10, 20$ and 50 GeV^2 in a wide range of x is excellent. In Fig.5, we compared the gluon distribution results with and without considering the rescaling variable of x at $Q^2 = 10$ and 20 GeV^2 with an analytical solution using a Froissart bounded structure function $F_2(x, Q^2)$ in Ref.[37] by M. M. Block, L. Durand and Douglas W. McKay (BDM). We observe that the results with the rescaling variable is comparable with those using the Froissart-bound type parametrization of the proton structure function.

CONCLUSIONS

The manuscript focuses on three interconnected topics: the study of the ratio $F_{L2}(x, Q^2) = F_L(x, Q^2)/F_2(x, Q^2)$, the calculation of the reduced cross section in momentum space using the Block-Durand-Ha (BDH) parameterization of the proton structure function $F_2(x, Q^2)$ and the leading-order (LO) longitudinal structure function $F_L(x, Q^2)$, and the evaluation of the gluon distribution function $G(x, Q^2)$.

We have developed a method for the analytical solution of the longitudinal structure function based on the proton structure function at low- x in the momentum-space approach. The momentum space evolution of the longitudinal structure function relies on the Froissart-bounded parametrization of the DIS structure function $F_2(x, Q^2)$ within the leading-order approximation.

The extraction procedure has been elaborated for an analysis of the ratio of structure functions, $F_{L2}(x, Q^2) = \frac{F_L(x, Q^2)}{F_2(x, Q^2)}$ in the kinematical region of the H1 collaboration data. The momentum space evolution of the ratio of structure functions is entirely determined by the effective parameters of the BDH parametrization and compared with the CDP bounds. The study further examines the ratio $F_{L2}(x, Q^2)$, comparing it to H1 data and bounds from the color dipole model, finding strong agreement that supports the proposed methods.

We have applied the developed method to extract the reduced cross section in the momentum-space approach within the kinematical conditions corresponding to that available at the HERA collider. The results are validated

against HERA data and extended to the Large Hadron Electron Collider (LHeC) domain. We have performed an analysis of the x -evolution of the extracted of the gluon distribution function in momentum-space approach. It has been demonstrated that the gluon distribution function $G(x, Q^2)$ is evaluated in momentum-space approach and compared to NNPDF3.0LO gluon structure functions, demonstrating excellent agreement for moderate Q^2 values within the range $10^{-5} \leq x \leq 1$. Such an analysis can be accomplished by employing the charm quark mass in the rescaling variable (which is directly related to the gluon density in the photo-gluon fusion reactions) as a useful tool for estimations of the gluon distributions in comparison with other results.

In summary, our calculation of the reduced cross section in momentum-space approach employs the Block-Durand-Ha parameterization for the proton structure function $F_2(x, Q^2)$ and the LO longitudinal structure function $F_L(x, Q^2)$, as proposed by Boroun and Ha, utilizing Laplace transform techniques. We have benchmarked our reduced cross section results against the H1 data and extrapolated them into the LHeC domain. Furthermore, the ratio $F_{L2}(x, Q^2)$ derived from our analysis is compared with both the H1 data and the CDP bounds, showing consistency. Lastly, our evaluation of the gluon distribution functions $G(x, Q^2)$ in momentum-space approach corroborates the NNPDF3.0LO gluon distribution functions for moderate Q^2 values within the range $10^{-5} \leq x \leq 1$. The results not only are comparable with the NNPDF3.0LO gluon distribution functions but also serve the Froissart-bound type parametrization of the proton structure function.

ACKNOWLEDGMENTS

Authors would like to thank Professor Loyal Durand for useful comments and invaluable support.

APPENDIX A

COLOR DIPOLE MODEL

In the color dipole model (CDM), the virtual photon γ^* exchanged between the electron and proton currents with virtuality Q^2 , split into a quark-antiquark pair (a dipole) which then interacts with the target proton via gluon exchanges [17]. The dipole picture for DIS is used to describe the data at low and moderate values of Q^2 , as shown in the various applications of the dipole model in Refs. [18–24]. The total γ^*p cross section is given by

$$\sigma_{L,T}^{\gamma^*p}(x, Q^2) = \sum_f \int d^2\mathbf{r} \int_0^1 dz |\Psi_{L,T}(\mathbf{r}, z; Q^2)|^2 \sigma_{\text{dip}}(x, \mathbf{r}), \quad (12)$$

where the sum over quark flavours f is performed. The quark and antiquark in this dipole carry a fraction z and $1 - z$ of the photon longitudinal momentum respectively, and the transverse size between the quark and antiquark is given by the vector \mathbf{r} . Here $\Psi_{L,T}(\mathbf{r}, z; Q^2)$ are the appropriate spin averaged light-cone wave functions of the photon, which give the probability for the occurrence of a $(q\bar{q})$ fluctuation of transverse size with respect to the photon polarization.

The measured structure functions F_2 and F_L are related to the dipole cross section σ_{dip} by

$$F_2(x, Q^2) = \frac{Q^2}{4\pi^2\alpha_{\text{em}}} (1 - x) \sum_f \int d^2\mathbf{r} \int_0^1 dz \left[|\Psi_T(\mathbf{r}, z; Q^2)|^2 + |\Psi_L(\mathbf{r}, z; Q^2)|^2 \right] \sigma_{\text{dip}}(x, \mathbf{r}), \quad (13)$$

and

$$F_L(x, Q^2) = \frac{Q^2}{4\pi^2\alpha_{\text{em}}} (1 - x) \sum_f \int d^2\mathbf{r} \int_0^1 dz |\Psi_L(\mathbf{r}, z; Q^2)|^2 \sigma_{\text{dip}}(x, \mathbf{r}). \quad (14)$$

The ratio of structure functions is defined by the following form

$$F_{L2}(x, Q^2) = \frac{\sum_f \int d^2\mathbf{r} \int_0^1 dz |\Psi_L(\mathbf{r}, z; Q^2)|^2 \sigma_{\text{dip}}(x, \mathbf{r})}{\sum_f \int d^2\mathbf{r} \int_0^1 dz \left[|\Psi_T(\mathbf{r}, z; Q^2)|^2 + |\Psi_L(\mathbf{r}, z; Q^2)|^2 \right] \sigma_{\text{dip}}(x, \mathbf{r})}. \quad (15)$$

In Refs.[22, 23, 25], authors show that at large Q^2 , the ratio of photo absorption cross sections is determined by a parameter ρ that describes the dissociation of photons into $q\bar{q}$ pairs, $\gamma_{L,T}^* \rightarrow q\bar{q}$, with

$$R = \frac{1}{2\rho}, \quad (16)$$

where the factor 2 originates from the difference in the photon wave functions. Indeed, the ρ parameter describes the ratio of the average transverse momenta $\rho = \frac{\langle \vec{k}_\perp^2 \rangle_L}{\langle \vec{k}_\perp^2 \rangle_T}$, or it can be related to the ratio of the effective transverse sizes of the $(q\bar{q})_{L,T}^{J=1}$ states as $\frac{\langle \vec{r}_\perp^2 \rangle_L}{\langle \vec{r}_\perp^2 \rangle_T} = \frac{1}{\rho}$. For the parameter $\rho = \frac{4}{3}$ in Ref.[23] ⁷, one can find that $R = \frac{3}{8} = 0.375$ and the ratio of structure functions is $F_{L2}(x, Q^2) = \frac{3}{11} = 0.273$. For the specific value $\rho = 1$ (i.e., helicity independent), this ratio is $\simeq 0.34$ which is an upper bound for $F_{L2}(x, Q^2)$ in the dipole model.

In Refs.[26–28], authors show that the ratio of structure functions in the dipole model is independent of the dipole cross section σ_{dip} . Indeed, it is proportional to the photon- $q\bar{q}$ wave function as

$$F_{L2}(x, Q^2) = g(Q, r, m_q) \leq \tilde{g}(z_m) = 0.27139, \quad (17)$$

where

$$g(Q, r, m_q) = \frac{\int_0^1 dz |\Psi_L(\mathbf{r}, z; Q^2)|^2}{\int_0^1 dz \left[|\Psi_T(\mathbf{r}, z; Q^2)|^2 + |\Psi_L(\mathbf{r}, z; Q^2)|^2 \right]} \quad (18)$$

and m_q is the mass of the active quark ⁸. For massless quarks, the function $g(Q, r, m_q)$ is defined by the dimensionless variable $z = Qr$ as the function $\tilde{g}(z) = g(Q, r, 0)$ has a maximum at $z_m = 2.5915$ with $\tilde{g}(z) = 0.27139$. It was shown in literature [29–32] that, for all $Q \geq 0$, $r \geq 0$ and $m_q \geq 0$, the bound specified by Eq. (17) for the ratio of structure functions is also valid.

APPENDIX B

Let us start with the series in Eq. (6):

$$S(v) = \sum_{k=1}^{\infty} \frac{k}{(k+1)^2 - 3(k+1) + 4} e^{-(k+1)v} = \sum_{m=1}^{\infty} \frac{m-1}{m^2 - 3m + 4} e^{-mv}. \quad (19)$$

For large m , the terms in the series behave as e^{-mv}/m . Noting that

$$\sum_{m=1}^{\infty} \frac{e^{-mv}}{m} = -\ln(1 - e^{-v}) = -\ln(1 - x), \quad (20)$$

we can subtract this series from Eq.(19) to get a series that converges as e^{-mv}/m^2 , so converges even as $v \rightarrow 0$, and add it back in as $-\ln(1 - e^{-v})$. This gives

$$S(v) = \sum_{m=1}^{\infty} \frac{2m-4}{m(m^2 - 3m + 4)} e^{-mv} - \ln(1 - e^{-v}). \quad (21)$$

The result also shows explicitly the divergence for $x = e^{-v} \rightarrow 1$ or $v \rightarrow 0$.

⁷ For further discussion, readers can refer to the papers by M. Kuroda and D. Schildknecht: "Phys. Rev. D 85 (2012) 094001" and "J. Mod. Phys. A 31 (2016) 1650157".

⁸ For further discussion see [27].

Let us denote

$$S_{\text{mod}}(v) = \sum_{m=1}^{\infty} \frac{2m-4}{m(m^2-3m+4)} e^{-mv}. \quad (22)$$

We can further improve the convergence of the series $S_{\text{mod}}(v)$ by subtracting the asymptotic series for m large and adding it back in as the dilogarithm $\text{Li}_2(e^{-v}) = \sum_{m=1}^{\infty} e^{-mv}/m^2$. This gives a series in which the remainder, after M terms, is of order $1/M^2$

$$S_{\text{mod}}(v) = \sum_{m=1}^{\infty} \left[\frac{2m-4}{m(m^2-3m+4)} - \frac{2}{m^2} \right] e^{-mv} + \text{Li}_2(e^{-v}). \quad (23)$$

In Fig. 6, we show the plots of $S(v)$ and $S_{\text{mod}}(v)$, given by Eq. (21) and Eq. (23), respectively, in a wide range of v . In both plots, the maximum of m in the series is chosen to be $M = 1000$ with a point wise accuracy $\sim 1/10^6$. For present purposes value $M \sim 50$ with accuracy $1/10^4$ or better is sufficient.

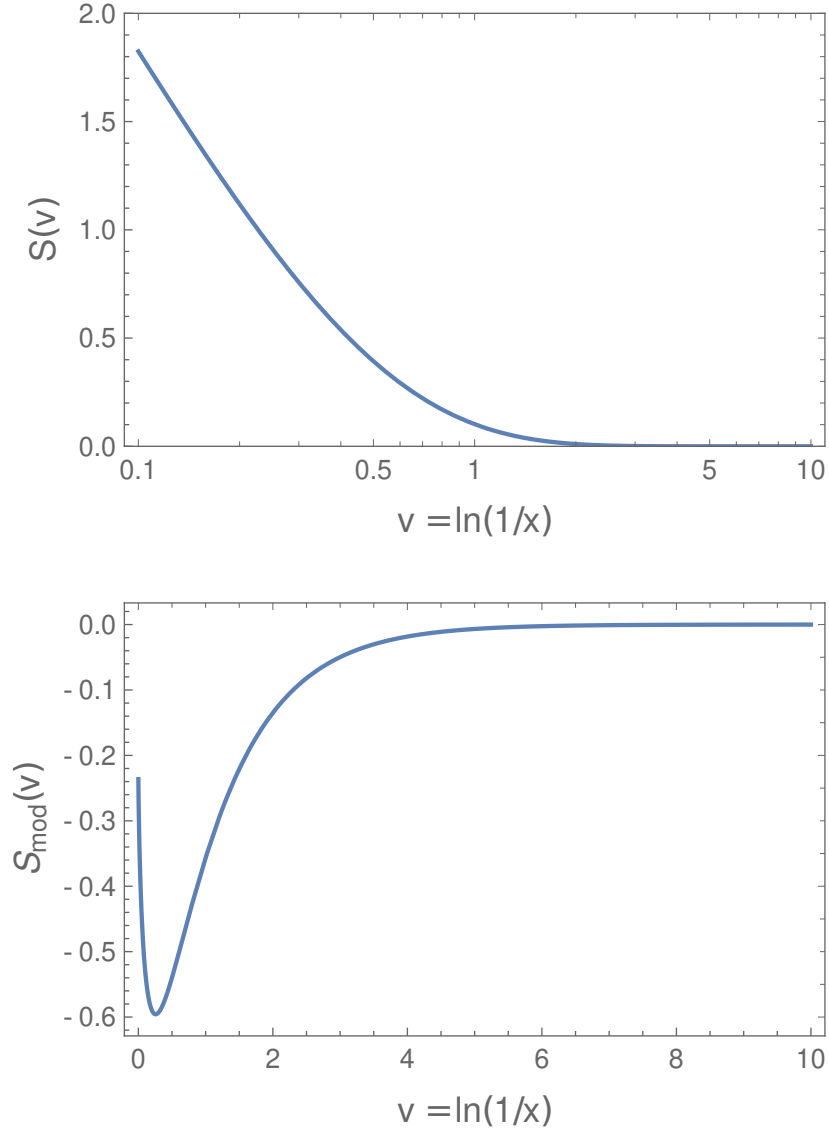


FIG. 6: Plots of $S(v)$ and $S_{\text{mod}}(v)$, given by Eq. (21) and Eq. (23), respectively, in a wide range of v . Note that $S_{\text{mod}}(0) = -0.2364$. In both plots, the maximum of m in the series is chosen to be $M = 1000$ with a point wise accuracy $\sim 1/10^6$.

TABLE I: The effective parameters in the BDH expression for $F_2(x, Q^2)$ in Eqs. (11) and (12) at small x for $0.15 \text{ GeV}^2 < Q^2 < 3000 \text{ GeV}^2$ provided by the following values. The fixed parameters are defined by the Block-Halzen fit to the real photon-proton cross section as $M^2 = 0.753 \pm 0.068 \text{ GeV}^2$, $\mu^2 = 2.82 \pm 0.290 \text{ GeV}^2$, and $a_{00} = 0.2550 \pm 0.016$ [9].

parameters	value
n	$n = 11.49 \pm 0.99$
λ	2.430 ± 0.153
a_{01}	$1.475 \times 10^{-1} \pm 3.025 \times 10^{-2}$
a_{10}	$8.205 \times 10^{-4} \pm 4.62 \times 10^{-4}$
a_{11}	$-5.148 \times 10^{-2} \pm 8.19 \times 10^{-3}$
a_{12}	$-4.725 \times 10^{-3} \pm 1.01 \times 10^{-3}$
a_{20}	$2.217 \times 10^{-3} \pm 1.42 \times 10^{-4}$
a_{21}	$1.244 \times 10^{-2} \pm 8.56 \times 10^{-4}$
a_{22}	$5.958 \times 10^{-4} \pm 2.32 \times 10^{-4}$

-
- [1] H1 Collab. (C.Adloff et al.), Eur.Phys.J.C 21 (2001) 33.
[2] S.Schmitt, Workshop on EW and BSM physics at the EIC(2020); K.Lipka, Standard model at the LHC (2013).
[3] J. Abelleira Fernandez, et al. [LHeC Collaboration], J. Phys. G 39 (2012) 075001.
[4] P.Agostini et al. [LHeC Collaboration and FCC-he Study Group], J. Phys. G: Nucl. Part. Phys. 48 (2021) 110501.
[5] M. Klein, arXiv:1802.04317[hep-ph].
[6] M. Klein, Ann. Phys. 528 (2016) 138.
[7] N. Armesto, et al., Phys. Rev. D 100 (2019) 074022.
[8] G.R.Boroun and B.Rezaei, Phys. Lett. B 816 (2021) 136274.
[9] M. M. Block, L. Durand and P. Ha, Phys.Rev.D 89 (2014) 094027.
[10] G.R.Boroun and P.Ha, Phys.Rev.D 109 (2024) 094037.
[11] Martin M. Block, Loyal Durand and Douglas W. McKay, Phys.Rev.D 79 (2009) 014031.
[12] Martin M. Block, Loyal Durand, Phuoc Ha and Douglas W. McKay, Phys.Rev.D 83 (2011) 054009.
[13] Martin M. Block, Loyal Durand, Phuoc Ha and Douglas W. McKay, Phys.Rev.D 84 (2011) 094010.
[14] Martin M. Block, Loyal Durand, Phuoc Ha and Douglas W. McKay, Phys.Rev.D 88 (2013) 014006.
[15] H1 Collab. (V. Andreev et al.), Eur.Phys.J.C 74 (2014) 2814.
[16] NNPDF Collaboration (Richard D. Ball et al.), JHEP 04 (2015) 040.
[17] N. N. Nikolaev and B. G. Zakharov, Phys. Lett. B 332 (1994) 184.
[18] N. N. Nikolaev and B. G. Zakharov, Z. Phys. C 49 (1991) 607.
[19] N. N. Nikolaev and B. G. Zakharov, Z. Phys. C 53 (1992) 331.
[20] K. Golec-Biernat and M. Wüsthoff, Phys. Rev. D 59 (1999) 014017; Phys. Rev. D 60 (1999) 114023.
[21] J. Bartels, K. Golec-Biernat and H. Kowalski, Phys. Rev. D 66 (2002) 014001.
[22] G. Cvetic, D. Schildknecht, B. Surrow and M. Tentyukov, Eur. Phys. J. C 20 (2001) 77.
[23] M. Kuroda and D. Schildknecht, Phys. Lett. B 618 (2005) 84; Phys. Lett. B 670 (2008) 129; Phys. Rev. D 85 (2012) 094001; J. Mod. Phys. A 31 (2016) 1650157.
[24] G.R.Boroun, M. Kuroda and D. Schildknecht, arXiv[hep-ph]:2206.05672.
[25] D. Schildknecht and M. Tentyukov, arXiv[hep-ph]:0203028.
[26] C. Ewerz, A. von Manteuffel and O. Nachtmann, Phys.Rev.D 77 (2008) 074022.
[27] C. Ewerz, A. von Manteuffel, O. Nachtmann and A. Schoning, Phys.lett.B 720 (2013) 181.
[28] C. Ewerz, O. Nachtmann, Phys.Lett.B 648 (2007) 279.
[29] B.Rezaei and G.R.Boroun, Phys.Rev.C 101, (2020) 045202.
[30] M. Niedziela and M. Praszalowicz, Acta Physica Polonica B 46 (2015) 2018.
[31] G.R.Boroun and B.Rezaei, Phys.Rev.C 103, (2021) 065202; Nucl.Phys.A 990 (2019) 244.
[32] G.R.Boroun, Eur.Phys.J.A 57 (2021) 219; Phys.Rev.D 109 (2024) 054012.
[33] L.P. Kaptari, et al., Phys.Rev.D 99 (2019) 096019.
[34] M.A.G.Aivazis et al., Phys.Rev.D 50 (1994) 3102.
[35] G.Beuf, C.Royon and D.Salek, Eur. Phys. J. C 84 (2024) 84.

- [36] T. Lappi, H. Mantysaari, H. Paukkunen, and M. Tevio, Eur. Phys. J. C 84 (2024) 84.
- [37] Martin M. Block, Loyal Durand and Douglas W. McKay, Phys.Rev.D 77 (2008) 094003.